THE JOURNAL OF PHYSICAL CHEMISTRY B
A JOURNAL OF THE AMERICAN CHEMICAL SOCIETY

pubs.acs.org/JPCB

Article

Activation-Induced Reorganization of Energy Transport Networks in the β_2 Adrenergic Receptor

Published as part of The Journal of Physical Chemistry virtual special issue "125 Years of The Journal of Physical Chemistry".

Humanath Poudel and David M. Leitner*

Cite This: *J. Phys. Chem. B* 2021, 125, 6522–6531

Read Online

ACCESS | Metrics & More | Article Recommendations | Supporting Information

ABSTRACT: We compute energy exchange networks (EENs) through the β_2 adrenergic receptor (β_2AR), a G-protein coupled receptor (GPCR), in inactive and active states, based on the results of molecular dynamics simulations of this membrane bound protein. We introduce a new definition for the reorganization of EENs upon activation that depends on the relative change in rates of energy transfer across noncovalent contacts throughout the protein. On the basis of the reorganized network that we obtain for β_2AR upon activation, we identify a branched pathway between the agonist binding site and the cytoplasmic region, where a G-protein binds to the receptor when activated. The pathway includes all of the motifs containing molecular switches previously identified as contributing to the allosteric transition of β_2AR upon agonist binding. EENs and their reorganization upon activation are compared with structure-based contact networks computed for the inactive and active states of β_2AR.

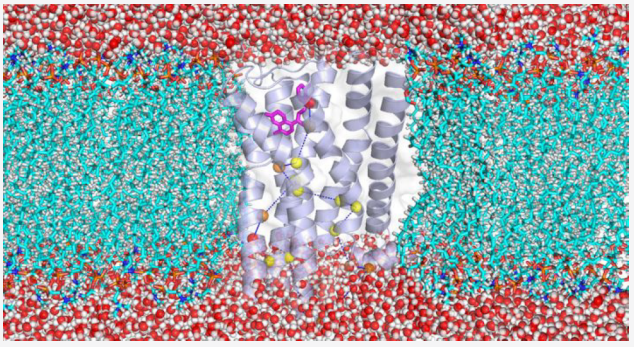

1. INTRODUCTION

Numerous methods have been developed to identify regions of proteins that respond to activation and facilitate allosteric transitions, with a goal of locating residues or groups of residues particularly critical to regulation.[1−5] Networks of dynamically coupled regions connecting distal binding sites have been identified and examined,[2−6] including networks of pathways for energy transport and signaling through proteins and protein complexes.[7−13] We present here results of molecular dynamics (MD) simulations of the β_2 adrenergic receptor (β_2AR), a G-protein-coupled receptor (GPCR), from which we have identified networks for energy transport through this membrane protein. Reorganization of the network during activation occurs as contacts between noncovalently bonded residues rearrange upon change of state. In particular, the rearrangement of the energy transport network during activation occurs predominantly in motifs,[14−16] groups of residues conserved in Class A GPCRs such as β_2AR, which contain the molecular switches that reorient and reorganize contacts between transmembrane (TM) helices.[17−19] A network defined in terms of the relative change in rates of energy transfer across noncovalent contacts upon activation reveals a branched pathway between the agonist binding region and the G-protein binding region that includes all of the previously identified motifs.

GPCRs mediate cellular responses from the exterior of the cell into the cytoplasm.[17−21] They contain seven TM helices, where each helix is connected to another either by an extracellular loop (ECL) or intracellular loop (ICL). The activation of many GPCRs from the inactive state to the active state is triggered by an agonist bound in the orthosteric site, leading to conformational changes in GPCRs via shifts in the TM helices.[16,22,23] In this study, we construct dynamic and contact networks for β_2AR in the inactive (antagonist bound) and active (agonist bound) states. β_2AR is a rhodopsin-like (Class A) GPCR functioning as neurotransmitter receptor.[23] It mediates many physiological functions such as smooth muscle relaxation and is a therapeutic target for asthma and cardiac diseases.[24] In Figure 1, the active-state (light blue) and inactive-state (green) structures are shown. Figure 1 depicts the outward movement of TM6 in the active state, one of the major hallmarks of GPCR activation, as well as a smaller outward movement of TM5 and inward movement of TM7.

Received: April 15, 2021
Revised: May 26, 2021
Published: June 9, 2021

Downloaded via David Leitner on June 24, 2021 at 18:07:11 (UTC).
See https://pubs.acs.org/sharingguidelines for options on how to legitimately share published articles.

ACS Publications

© 2021 American Chemical Society

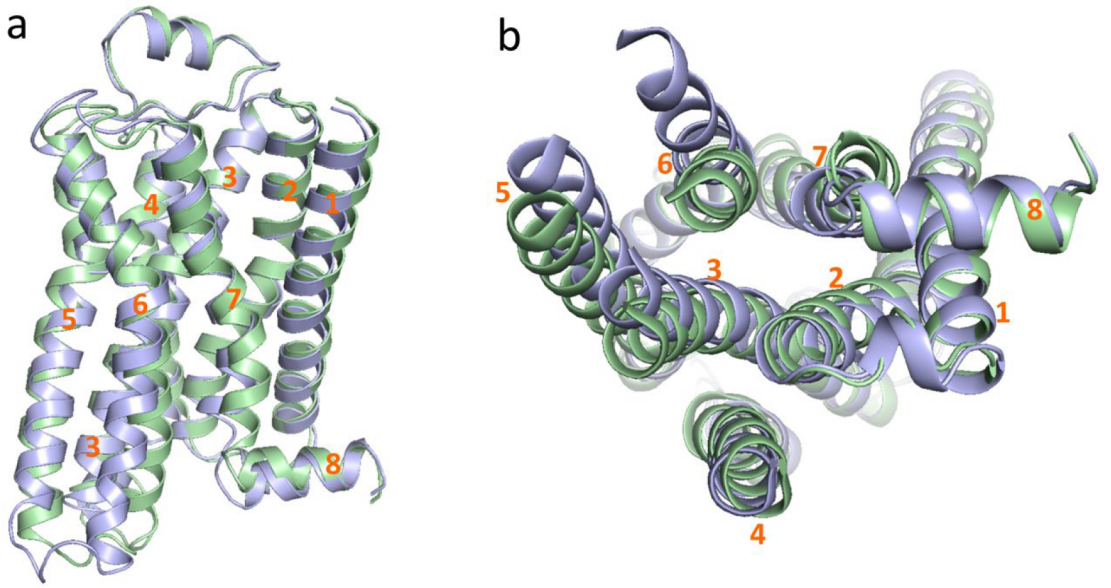

Figure 1. (a) Side view of β_2AR and (b) view from the cytoplasm. The active state (light blue) is superimposed on the inactive state (green). The intercellular loops ICL2 and ICL3 are not shown in the figure to more clearly depict shifts in positions of helices. The seven TM helices and an eighth helix in the cytoplasm are labeled.

A variety of networks, including structure-based contact networks,[1,25−28] dynamic perturbation networks,[4] and energy transport networks[7,9,29,30] have been defined and studied to identify regions of a protein, including water,[9,10,31−34] that play key roles in signaling and allosteric regulation. We focus on energy transport and contact networks in this study. Energy transport networks in proteins identify pathways by which proteins respond to photoexcitation and chemical reactions.[8,12,35] They have been computed at all-atom and at coarse-grained levels.[12] Networks of residues that transport energy have been obtained via computation of local energy diffusion coefficients,[36−41] estimated from the results of normal-mode analysis and related to thermal transport coefficients,[42−44] as well as computation of local energy currents obtained from time-correlation functions of the energy flux between residues.[7,35,45] We carry out the latter approach, developed by Yamato and co-workers, in this study. Energy exchange networks (EENs)[7,45] are obtained as the intersection of relatively large rates of energy transfer between residues.[7,45] The rates of energy transfer are related to the equilibrium dynamics of the contacts[32,40,46−52] and can be measured by a number of time-resolved spectroscopic techniques.[53−58] We note that at such a coarse-grained level master equation simulations have modeled well the transport of energy when compared with the results of all-atom nonequilibrium MD simulations.[50,51]

We compute EENs for β_2AR in the inactive state, in which an antagonist is bound, and for the agonist-bound active state. Changes in EENs for the two states reflect changes in the interactions between residues that mediate energy transfer between them. Ota and Yamato, in their study of the oxygen sensor protein FixLH, have shown that these changes can indicate pathways by which allosteric transitions occur.[7] We follow their approach here and examine changes in EENs for the transition from inactive to active states of β_2AR. We find that the pathways generated by these changes include many of the motifs identified in earlier work as involved in the inactive-to-active transition. However, we also find that some are missing, in particular a motif containing side chains interacting via van der Waals contacts, across which rates of energy transfer are typically much smaller than across polar or charged contacts.[48]

We thereby consider an alternative criterion for quantifying the reorganization of the network upon activation, namely changes in the relative, rather than absolute, values of the rates of energy transfer. In this case rates of energy transfer across van der Waals contacts that may be larger in one state but significantly smaller in another can be accounted for even if such rates are relatively small compared to rates of energy transfer across polar contacts that rearrange during the inactive-to-active transition. Even if a change in rate of energy transfer across a van der Waals contact upon activation is small, the relative difference may not be small. We find by examining the relative changes in the EENs of β_2AR upon activation that all motifs containing molecular switches are included along a branched pathway from the agonist binding pocket to the cytoplasmic G-protein binding region. The energy transport networks computed for β_2AR are compared with contact networks based on structure, which we also compute.

In section 2 we provide information about the computational methods. In section 3 we present results and discuss the analysis of energy transport networks in β_2AR and their reorganization upon activation. Conclusions are provided in section 4.

2. COMPUTATIONAL DETAILS

The initial structure of β_2AR was obtained from the protein data bank (PDB) structure 3P0G, including the agonist ligand BI-167107 ($C_{21}H_{26}N_2O_4$). For the inactive state, we adopted the coordinates of PDB 2RH1, including the antagonist Carazolol ($C_{18}H_{22}N_2O_2$). The T4-lysozyme chimera of the inactive state was omitted, and the missing intercellular loop (ICL3) was modeled by using Modeller9.23.[59] Similarly, the missing residues of ICL3 of the active state were modeled by using the same program. With these adjustments both states consist of the same residue sequence. We set up the initial

https://doi.org/10.1021/acs.jpcb.1c03412
J. Phys. Chem. B 2021, 125, 6522−6531

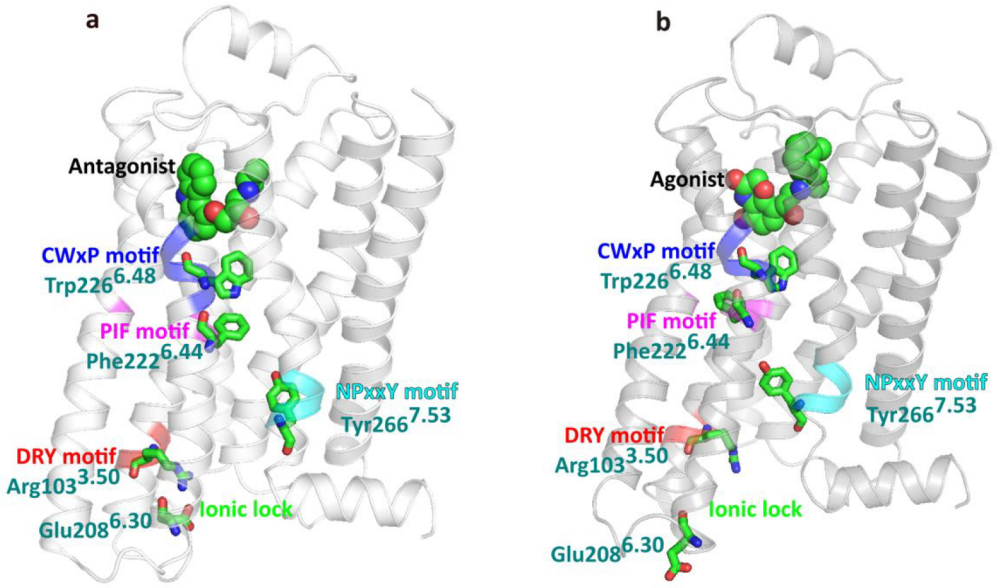

Figure 2. Motif regions and switches of β_2AR in (a) the inactive state and (b) the active state. Each motif region is indicated in a distinct color, which is the same for inactive and active states. Side chains that act as molecular switches during activation and the ionic lock are indicated.

systems using the CHARMM-GUI online interface,[60] which introduces any missing hydrogen atoms in the PDB. Each system was set up in a rectangular box embedded with 150 1-palmitoyl-2-oleoyl-*sn*-glycero-3-phosphocholine (POPC) lipid molecules to model the cell membrane and about 6000 water molecules. The systems were neutralized by using Na^+ and Cl^- ions with a final concentration of 0.15 M NaCl. We performed all simulations with the AMBER16 MD software package using the AMBER ff14SB force field for proteins,[61] the TIP3P model for water molecules, and the Lipid17 force field for lipids.[62]

For each state, we performed an energy minimization of 20000 steps employing the steepest descent method for the first 10000 steps and the conjugant gradient method for the remaining steps. Periodic boundary conditions were applied for all simulations. Following minimization, the system was heated as an NVT ensemble with a Berendsen thermostat,[63] starting from 0.1 to 300 K for 1 ns and held at 300 K for an additional 1 ns. Positional restraints were applied to the protein backbone atoms by using a force constant of 1 kcal/(mol Å^2). To constrain all hydrogen-containing bonds, the SHAKE algorithm was applied. The systems were equilibrated for 10 ns by applying positional restraints on protein backbone atoms with a force constant of 1 kcal/(mol Å^2) followed by another 20 ns without positional restraints. For both states, we performed 100 ns sampling simulations under an NPT ensemble. The trajectory files were saved each nanosecond for the next microcanonical (NVE) simulations. Snapshots from 51 to 100 ns were adopted for NVE simulations to compute energy currents. During this time the range of structures was the same as that found over similar intervals at earlier times. For instance, between 30 and 80 ns the standard deviation in the root-mean-square deviation (RMSD) in structure was found to be 0.08 and 0.12 Å for the inactive and active states, respectively, the same standard deviation in RMSD as found between 50 and 100 ns. Each NVE simulation was performed for 150 ps, with an integration time of 0.5 fs. The coordinates were saved every 5 fs, and the velocities were saved every 1 fs. To reduce the energy drift, an Ewald sum tolerance of 10^{-7} was selected.

The local energy conductivity was computed by using the CURrent calculation for Proteins (CURP) ver. 1.2.1,[45] developed by Yamato and co-workers. The local energy conductivity is defined as follows: Starting with the atom−atom energy flow,[45,64] $J^k_{i\leftarrow j} = {}^1/_2(\mathbf{v}_i\cdot\mathbf{F}_{ij} - \mathbf{v}_j\cdot\mathbf{F}_{ji})$, where $J^k_{i\leftarrow j}$ is the inter-residue atom−atom energy flow, mainly vibrational, between atoms i and j for trajectory k, $\mathbf{v}$ is the velocity, and $\mathbf{F}$ is the force of one atom on the other. The inter-residue energy flow is[45] $J^k_{A\leftarrow B}(t) = \sum_{j\in A}^{N_A}\sum_{j\in B}^{N_B} J^k_{i\leftarrow j}(t)$, where N_A (N_B) is the number of atoms in residue A (B). To determine energy currents, L_{AB}, for each pair of residues, we compute[45] $L^k_{AB} = \frac{1}{RT}\lim_{\tau\to\infty}\int_0^\tau \langle J^k_{A\leftarrow B}(t_0) J^k_{A\leftarrow B}(t+t_0)\rangle\, dt$, where R is the gas constant and T the temperature. We multiply L_{AB} by RT and report values in (kcal mol^{-1})^2 ps^{-1}, yielding G_{AB}, where $G_{AB} = (RT)L_{AB}$, termed the energy conductivity. We drop subscripts AB in the following. For a residue with excess energy, G quantifies the net energy transferred (multiplied by RT) across a nonbonded contact per unit time. An autocorrelation function window of 25 ps was chosen, which is well beyond the ∼1 ps observed correlation time. In total, we performed 50 NVE simulations for each of the states.

From this data, the energy conductivity for each residue−residue pair was averaged to evaluate the energy exchange networks[7,45] (EENs) for each state and the difference in energy exchange networks ΔEEN between the states, where the difference is defined as the change in the EEN going from inactive to active state. We also computed the relative difference in energy exchange networks (rΔEEN), defined for a particular contact as

$$r\Delta\mathrm{EEN} = \frac{G_{\mathrm{active}} - G_{\mathrm{inactive}}}{G_{\mathrm{active}} + G_{\mathrm{inactive}}} \quad (1)$$

where G_{active} and G_{inactive} correspond to the average G values for a residue pair in the active and inactive states, respectively, and the full rΔEEN map includes all contacts. To evaluate rΔEEN, a threshold of G > 10 (kcal mol^{-1})^2 ps^{-1} was selected to exclude very small rates, which can appear as noise in the calculations.[48] Finally, we obtained distance maps by

https://doi.org/10.1021/acs.jpcb.1c03412
J. Phys. Chem. B 2021, 125, 6522−6531

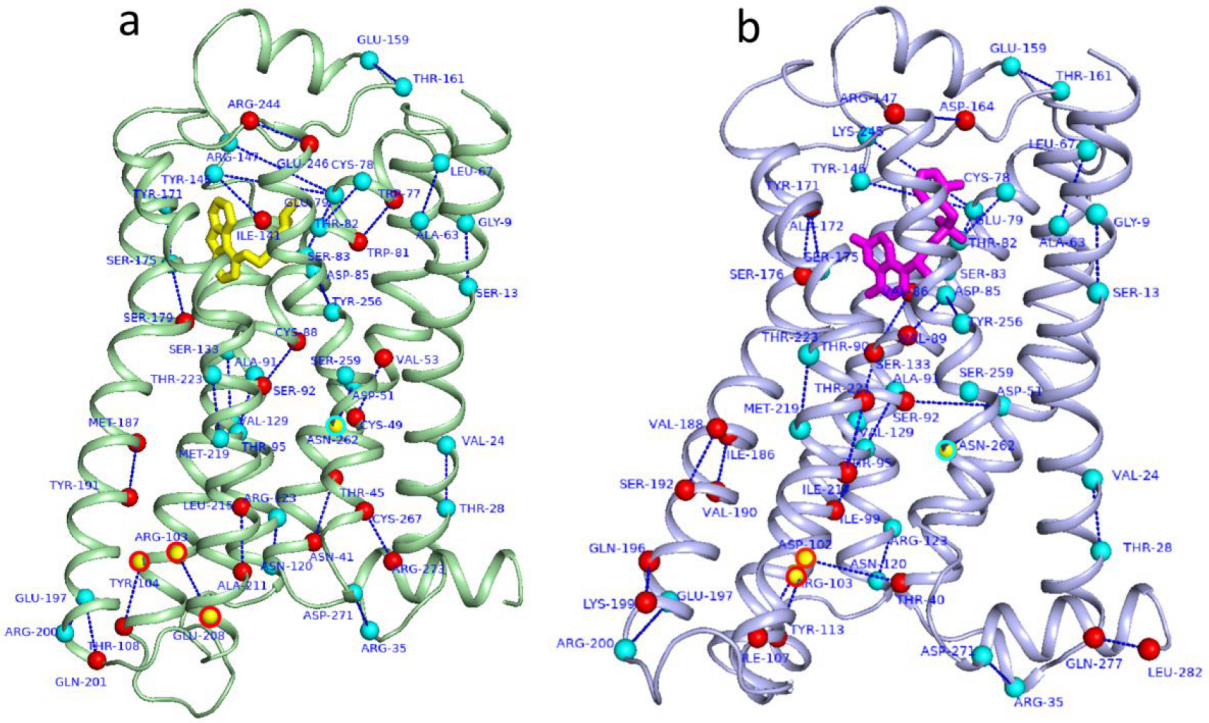

Figure 3. Residues of contacts for which G is relatively large (see text) in EENs for the (a) inactive state and (b) active state. Ribbon colors for the two states are as in Figure 1. Residue−residue pairs are connected by dotted lines. Cyan indicates residues in contacts common to both states, red indicates those unique to each state, and yellow indicates the residues in motif regions, circled by red or cyan to identify if they are unique to a state or common to both states.

computing the minimum distance between residue pairs of both inactive and active states of β_2AR from the 51−100 ns portion of NPT simulation that we sampled for the CURP calculations. The minimum distance is a Euclidean distance representing the closest pair of atoms between two residues. In total, 50 frames were taken at each nanosecond of the simulation, the minimum distance between each residue−residue pair computed for that frame, from which the average over all frames was computed to determine all inter-residue distances from the results of the MD simulations.

3. RESULTS AND DISCUSSION

We will be comparing energy transport networks computed for the inactive and active states of β_2AR with earlier work that has identified key residues in the transition from inactive to active states, which we turn to first. GPCRs consist of molecular switches, i.e., side chains that change orientation upon activation, found in conserved motifs across the transmembrane helices.[14,16,27] Motifs of Class A GPCRs, and β_2AR in particular, are shown in Figure 2. The DRY (Asp-Arg-Tyr) motif, in the cytoplasmic region of TM3, is involved in binding of the G-protein in the active state, where Arg acts as a switch forming an ionic lock with Glu208 of TM6, which is disrupted in the active state, that is, to fully activate the GPCR and bind the G-protein the lock first breaks.[18] The CWxP (Cys-Trp-x-Pro, where x is any residue) motif in TM6, the bottom of the ligand-binding pocket, consists of the switch Trp, which toggles in the active state closing the ligand-binding pocket. The NPxxY (Asn-Pro-x-x-Tyr) motif is in TM7, where Tyr rotates between different conformations. The PIF (Pro-Ile-Phe) motif is in TM4, TM5, and TM6, where Phe reorients between conformations upon activation. The motifs, switches, ionic lock of Arg103−Glu208 between TM3-TM6, and ligands in the inactive and active states are shown in Figure 2. Superscripts on the labels of switches follow the Weinstein numbering system.[65]

This study reports signaling pathways in β_2AR using energy exchange networks (EENs) and examining overlap with motif regions and switches indicated in Figure 2. EENs, ΔEENs, and rΔEENs, defined in the previous section facilitate identification of signaling in β_2AR and changes in signaling upon activation. While such changes are captured by ΔEENs, we consider in addition rΔEENs, or the relative change in networks between the states. The latter can capture effects of changes in the rates of energy transfer across van der Waals contacts sometimes missing in ΔEENs. Rates of energy transfer across van der Waals contacts are typically much smaller than across polar contacts,[48] so that the absolute difference in G corresponding to a change in state can also be small. However, the relative change may not be small. Hence, by using the rΔEEN, we can capture significant changes in energy transfer across a variety of contacts of the protein upon activation.

Contacts contributing most significantly to the EENs for the active and inactive states of β_2AR are plotted in Figure 3 and listed in Table S1. A more complete set of contacts contributing to the EENs of both states, including those with relatively small values of G, are plotted in Figure S1. Residues forming contacts that do not change upon activation are indicated in Figure 3 in cyan. Those contacts are largely found within individual helices. Changes upon activation arise primarily from interactions between helices, as the interhelix region is more flexible than regions within helices, as observed for other proteins.[66] For instance, notable differences occur due to an outward shift of TM6 and a smaller shift of TM5 and

https://doi.org/10.1021/acs.jpcb.1c03412
J. Phys. Chem. B 2021, 125, 6522−6531

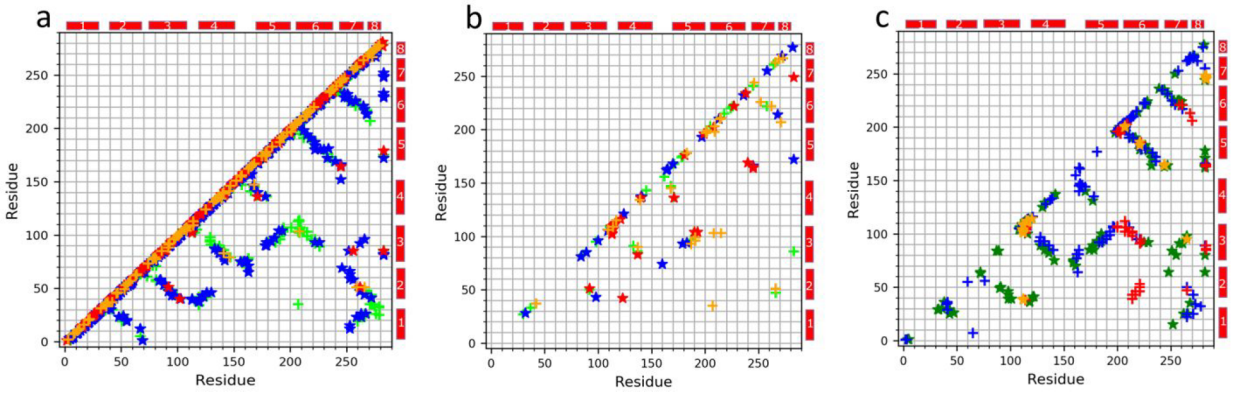

Figure 4. (a) Plot of ΔEEN ($G_{active} - G_{inactive}$): (blue ★) 2−60 (kcal mol^{-1})^2 ps^{-1}, (red ★) >60 (kcal mol^{-1})^2 ps^{-1}, (lime +) −2 to −60 (kcal mol^{-1})^2 ps^{-1}, and (orange +) <−60 (kcal mol^{-1})^2 ps^{-1}. (b) Plot of rΔEEN (eq 1): (blue ★) 0.7−0.9, (red ★) >0.9, (lime +) −0.9 to −0.7, and (orange +) <−0.9. (c) Plot of Δd, difference in distance map ($d_{active} - d_{inactive}$): (green ★) is Δ$d$ from −0.5 to −3.5 Å, (orange ★) <−3.5 Å, (blue +) 0.5−3.5 Å, and (red +) >3.5 Å. Residue numbers are indicated on the axes, and TM helices are labeled in the sidebar.

TM7 during activation. Similar movements of those helices are observed in prior studies of the same receptors.[17,67,68] In the inactive state, there are more contacts that give rise to facile energy transfer between TM3 and TM6, which disappear upon activation. Rapid energy transfer across the salt bridge Arg103−Glu208 between TM3 and TM6 in the inactive state is disrupted upon activation, an important step in the activation process.[17,20,67] The outward motion of TM6 during activation also causes disruption of energy transfer between it and TM1 as well as TM2, notably Arg35−Lys207 and Asp51−Phe222. Phe222 contributes to a switch (Figure 2) and reorients upon activation, moving away from Asp51.

Changes in EENs for the transition from inactive to active states, ΔEEN, the relative change upon activation (eq 1), rΔEEN, and changes in distance between residue pairs, Δd, are plotted in Figure 4, where residue pairs with relatively large contributions to each of these quantities are indicated. Consider first the ΔEEN (active−inactive) map plotted in Figure 4a, for which the values largest in magnitude are indicated there and in Table S2. Some of the contacts for which the difference in G upon activation is especially large and positive are associated with motifs plotted in Figure 2. The following are particularly noteworthy: Thr40−Asp102 and Asp51−Ser92 between TM2 and TM3, where Asp102 lies in the DRY motif. The contact Asp51−Asn262 is observed between TM2 and TM7, where Asn262 lies in the NPxxY motif. Moreover, Asp85−Tyr256 and Asp85−ligand are observed between TM3 and TM7 and between TM3 and the ligand, respectively. The contact Ser179−ligand is formed between TM5 and the ligand. It has been noted previously that a significant step in activation is breaking the Ser179−ligand contact.[67]

Contacts for which the difference in G upon activation is negative and the magnitude large include Asp51−Ser259 and Asp51−Tyr266 as well as interactions between TM2−TM7. Tyr266 (Y) lies in the NPxxY motif, shown in Figure 2, and acts as a switch that reorients upon activation. The contact Arg103−Glu208 between TM3 and TM6, also shown in Figure 2, stabilizes the outward motion of TM6 in the active state. Also noteworthy is the contact between Tyr104 of the DRY motif and Thr108 within the same helix.

We turn now to rΔEEN plotted in Figure 4b. The values largest in magnitude are indicated there and listed in Table S3. Large positive values include the following: Asp102−Tyr113, a contact between the DRY motif in TM3 and intercellular loop ICL2, as well as Tyr104 of the DRY motif and Val190 and Arg193 of TM5. The switch residue of the PIF motif, Phe222, interacts with Leu227 within TM6. Other contacts Thr136−Tyr171, Asp164−Lys145, Phe165−Lys245, and Gln169−Asp240 are formed in the extracellular region and close to the binding pocket. Ile149 forms an interaction with the ligand upon activation. There are generally more large positive changes seen in the rΔEEN than large negative changes near the ligand-binding site, corresponding to enhanced interactions and energy transfer between the ligand (agonist, as opposed to antagonist) and nearby residues upon activation.

Relatively large negative values in the rΔEEN map include the following contacts: Arg35−Lys207 between ICL1 and TM6 and Asp271−Lys207 between TM7 and TM6, even as the latter are quite far apart in distance. Also in this category is Asp51−Tyr266, between TM2 and TM7, consistent with the reorienting of Tyr266, a switch of the NPxxY motif, as shown in Figure 2. Another notable contact in this category is the salt bridge between Arg103−Glu208, termed the lock in Figure 2, which opens upon activation allowing TM6 to move outward. The switch residue Phe222 of the PIF motif appears in the contact Phe222−Asn262, where Asn262 is a residue in the NPxxY motif. This interaction between two motifs is disrupted, resulting in the larger relative (negative) change during activation. Similarly, Trp226 of the CWxP motif, a switch shown in Figure 2, appears in contact with Asn252. Negative changes in the rΔEEN map for contacts between Ile93−Met187, Ile of the PIF motif, and Arg103−Leu215, Arg103 of the DRY motif, are also observed.

Changes in the distance map, Δd (active − inactive), are plotted in Figure 4c. This map is based on distance maps for each state plotted in Figure S2; values of the minimum distance, d, between residue pairs for each state, used to calculate the differences plotted in Figure 4c, are discussed below. We observe a region where distances increase upon activation between TM6 and TM3, TM2, and TM7. On the other hand, there is a region where distances become smaller upon activation, between the TM7−TM3, indicating the movement of TM7 toward TM3. We also see, near the binding site, that residues are closer to the agonist in the active state than to the antagonist in the inactive state.

Contacts indicated in Figure 4 are plotted with protein structures in Figure 5. Residue pairs for which changes in G,

https://doi.org/10.1021/acs.jpcb.1c03412
J. Phys. Chem. B 2021, 125, 6522−6531

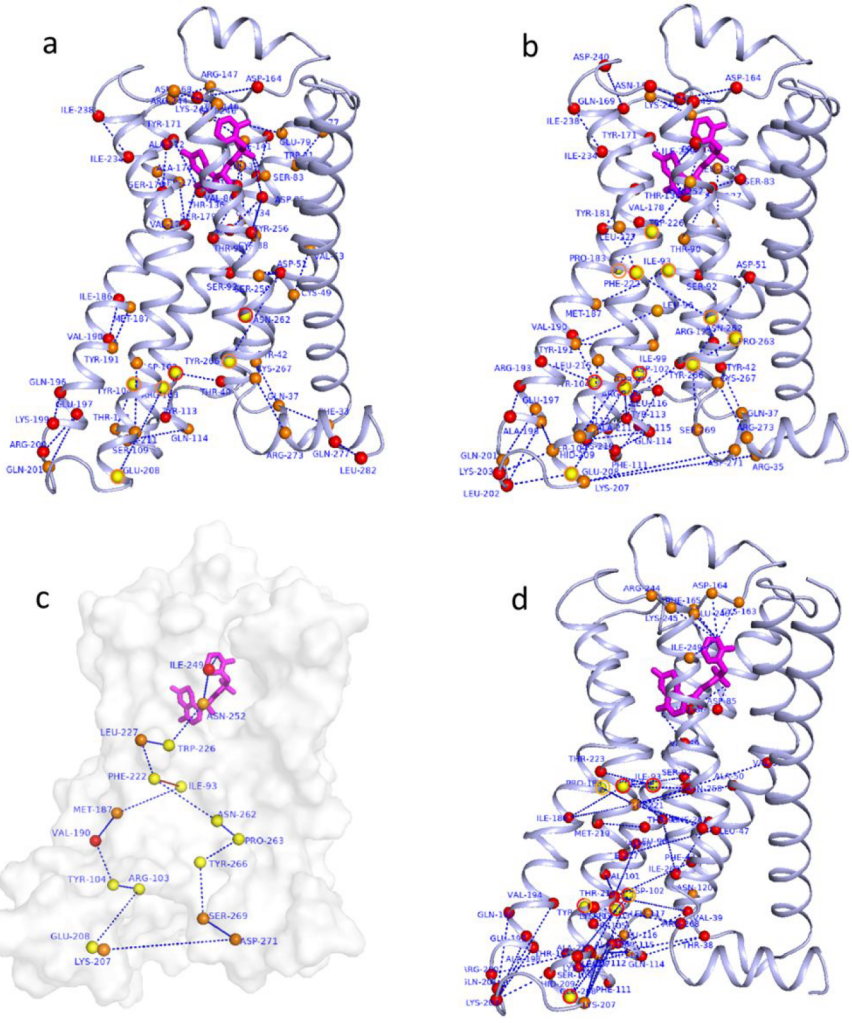

Figure 5. (a) Contacts from ΔEEN map. Residues of contacts with $\Delta G > 60$ (kcal mol^{-1})^2 ps^{-1} are indicated in red and $\Delta G < -60$ (kcal mol^{-1})^2 ps^{-1} in orange. Yellow indicates residues of motifs containing switches; red and orange circles denote those with positive and negative ΔG, respectively. (b) Contacts from $r\Delta$EEN. Residues of contacts with values >0.9 are indicated in red and <−0.9 are indicated in orange; yellow is as in (a). (c) Diagram of signaling pathways of β_2AR obtained from (b), where dotted lines indicate contacts present in (b) and solid lines contacts less than 3 positions apart in sequence; red indicates residue forming a contact falling just below threshold but within the same motif. (d) Networks formed by Δd, where red indicates values >3.5 Å, orange values <−3.5 Å, and the yellow is as in (a) and (b).

relative changes in G, or change in distance, d, are large in magnitude are indicated in Figure 5 using the same color scheme as in Figure 4. An exception is if a residue belongs to one of the motifs plotted in Figure 2. Those residues are indicated in yellow, circled in red or orange to indicate positive or negative differences, as in Figure 4. Though the number of residues obtained from each kind of difference map indicated in Figure 5 is comparable, we find that the $r\Delta$EEN map contains the most residues belonging to the motifs plotted in Figure 2. The ΔEEN map plotted in Figure 5a contains six such residues while the $r\Delta$EEN map plotted in Figure 5b contains 11. Indeed, for the $r\Delta$EEN map we find that each motif is represented, with at least one residue of each switch. No other map we have examined provides this.

Networks of contacts that appear in the $r\Delta$EEN map are plotted in Figure 5c, where one pathway from the agonist-binding region that branches into two before reaching the cytoplasmic region is observed. Large relative changes in the EENs between the inactive and active states are shown by using dotted lines and the residues that fall within the helices less than 3 positions apart are connected, if necessary, by using solid lines. A red line appears between Phe222 and Ile93 to indicate a contact that falls just below the lower threshold for Figure 4b, included because the residues lie within the same motif. Indeed, prior studies indicate that change in the distance between Phe222−Ile93, also known as the connecter region, plays a key role in the activation of GPCRs.[67] Figure 5c not only illustrates the connection of the ligand to the cytoplasmic region via changes in the energy transport network that results during the transition from inactive to active states, it is also consistent with the reorientation of switches critical to that transition. From Phe222 we observe a branching of the pathway toward the cytoplasmic region. Along one branch, Phe222 of TM6 to Asn262 of the NPxxY motif triggers further changes in the motif and connects to Asp271. The interaction of Asp271 and Lys207 is long-range due to the charged groups and is involved in movement of TM6 from TM7. Along the other branch, Phe222 moves closer to Ile93 of TM3, which in turn interacts with Met187 of TM5. The nearby residue Val190 moves closer to Tyr104 of the DRY motif. Finally, the ionic lock between Arg103 to Glu208 is broken.

https://doi.org/10.1021/acs.jpcb.1c03412
J. Phys. Chem. B 2021, 125, 6522−6531

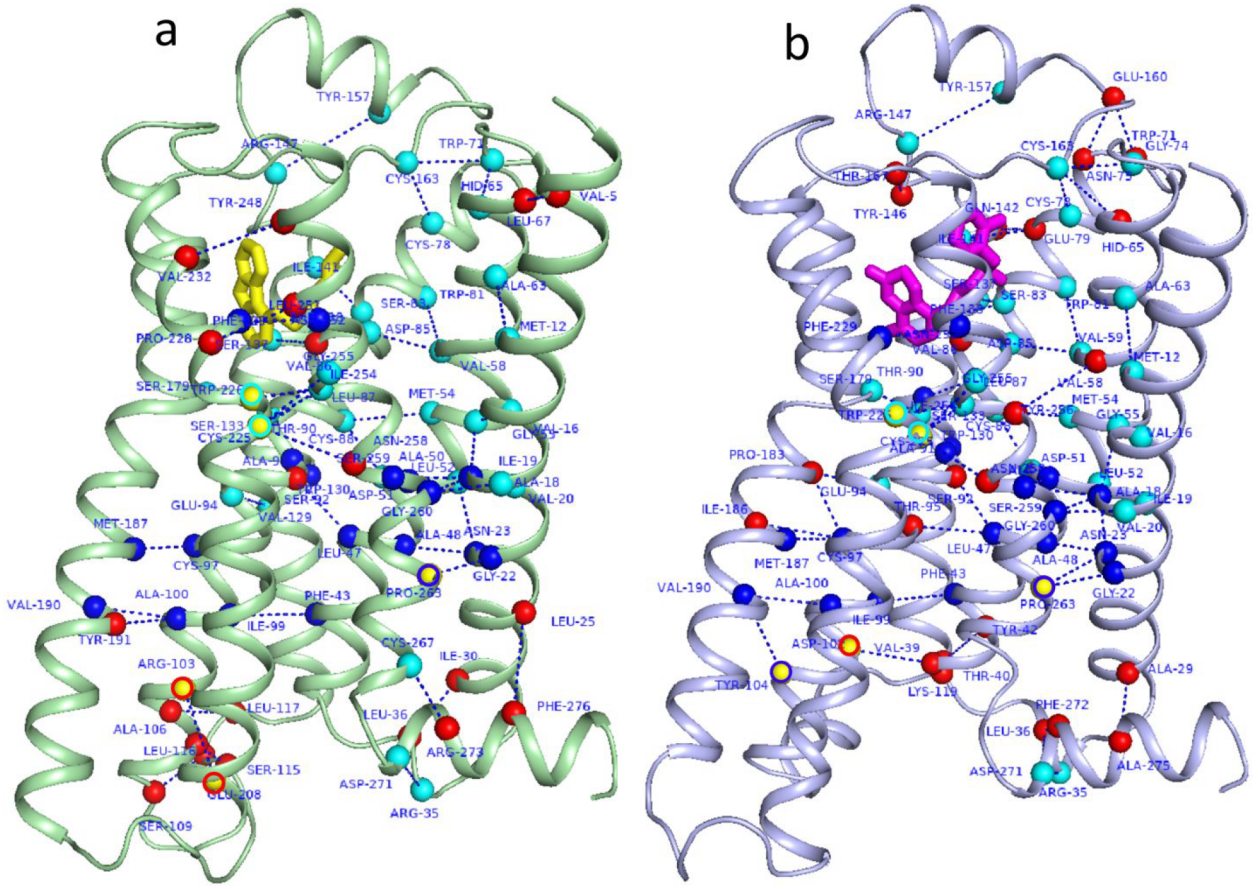

Figure 6. Distance maps for (a) the inactive state and (b) the active state. Ribbon colors for the two states are as in Figure 1. In both states, the residue pairs less than 4 Å are selected. The common contacts in both states are colored cyan. Consensus contacts[70] seen in the distance maps also are colored blue, and any other remaining contacts of the distance maps are colored red. Yellow indicates residues of motifs, as in other figures.

It is of interest to compare ΔEEN and *r*ΔEEN maps with changes in the contact map, that is, the Δ*d* map, plotted in Figure 4c and indicated on the protein in Figure 5d. There are many positive changes in distance upon activation, particularly between TM2 and TM6, which appear in the Δ*d* map, but such changes are less visible in the ΔEEN and *r*ΔEEN maps. For example, the contacts Val39−Thr214, Phe43−Thr214, Ser46−Ile217, and Ser46−Thr221 all change distance significantly. However, the corresponding change in the EENs is relatively small due to the small rate of energy transfer across these contacts in both states. The contacts Arg35−Lys207 and Lys207−Asp271 lie between ICL1−TM6 and TM7−TM6, respectively, and appear in the *r*ΔEEN, though they are not significant in the Δ*d* map, due to relatively large rates of energy transfer across charged contacts over sizable distances.[46−51] On the other hand, in the ΔEEN, we find the contacts Glu79−Tyr146 and Ser83−Ile141, between TM3 and TM4, exhibit a large negative change in rates of energy transfer upon activation but do not correspond to a large change in distance. This is due to changes in the orientation of the residues with respect to each other upon activation, altering the rate of energy transfer without much change in the inter-residue distance.

We also find important differences between the networks formed by contacts indicated by the ΔEEN and *r*ΔEEN maps plotted in Figures 5a and 5b and those formed by contacts in the Δ*d* map in Figure 5d. Most strikingly, the latter lacks a network connecting the extracellular and ligand-binding regions with the switches of the NPxxY motif. In contrast, the *r*ΔEEN in particular yields networks spanning the ligand-binding sites, switches, and the helices involved in activation.

Overall, while there is some correlation between *G* and minimum distance, *d*, between a pair of residues, there is significant variation in *G* for a given *d*. This observation has been made before in terms of the local energy diffusion coefficients between residues of proteins and the distance between them.[10,38,40] The relation between *G* and *d* for residue pairs of the inactive and active states is plotted in Figure S3 for noncovalent contacts. On average, *G* decreases with increasing *d*. However, for a given distance, *d*, there is large variation in *G*, which can span 2 orders of magnitude or more. We also observe *G* to be generally smaller for contacts that do not involve charged residues than those that do. Because there is some correlation between distance and rates of energy transfer between contacts, structure-based contact networks yield some of the insights into regions involved in allosteric transitions captured by dynamic network models. The energy transport networks, however, directly provide information about energy dynamics and signaling and, while somewhat correlated to distance, yield a more detailed description of the network of residues involved in activation. We have seen that for β_2AR the reorganization of energy transport networks upon activation, in particular *r*ΔEEN, captures all of the motifs containing molecular switches involved in activation.

Networks of charged residues of many Class A GPCRs including β_2AR have been identified in past work.[69] For β_2AR

https://doi.org/10.1021/acs.jpcb.1c03412
J. Phys. Chem. B 2021, 125, 6522−6531

they involve Asp51 (Asp79) of TM2, Asp81 (Asp113) of TM3, Cys267 (Cys327) of TM7, Asp 102 (Asp130), and Arg103 (Arg131) of the DRY motif, and Cys88 (Cys116) of TM3, all of which appear in the EENs we have computed. (The residue labels listed in parentheses are those listed in ref 69, the positions in the PDB, whereas the labels not in parentheses are in the sequence positions used in our study.) Only Cys225 (Cys285) found in ref 69 is absent in the EENs we have computed. Because we have included all interactions between residues in our analysis, we generate a more complete network for energy transfer in β_2AR. For example, the networks that we have identified include the van der Waals contacts that contribute to the structure of the PIF motif and lie along the pathways plotted in Figure 5c.

Prior studies of class A GPCRs including β_2AR have identified a conserved network of 24 contacts, termed a consensus network, which have been found to contribute to the stability of the GPCR fold.[70] The network was found by analysis by distance maps for Class A GPCRs. Of the 24 contacts, 20 contain at least one residue in TM1, TM2, and TM3, and overall they appear between helices TM1−TM2, TM3−TM4, TM3−TM5, and TM3−TM6−TM7. It is noteworthy that TM1 and TM2 do not undergo major changes in the activation process, indicating that the consensus network, important in stability, is quite distinct from networks of residues involved in activation. Indeed, the consensus contacts are formed in both inactive and active states of Class A GPCRs.[70] We have seen that reorganization of the energy transport networks upon activation captures the residues involved in activation quite well. We consider now whether the distance-based contact networks that we have computed better capture the consensus network.

Distance-based contacts are shown for inactive and active states in Figure 6. Because consensus contacts appear in both inactive and active states, we focus on those common to both states. In Figure 6 we highlight the common contacts and indicate those that have been identified in the past as parts of consensus networks.[70] We find 10 contacts to overlap the 24 contacts of the consensus network and another 13 contacts that lie close to, though not identical with, all but one of the remaining ones. The similar, though slightly shifted positions may be attributed to differences in the structures used to identify the contact network. In previous work the crystal structures were adopted whereas we have used structures from the MD simulations we have carried out. We note that contact networks, which suggest contacts important in stability of Class A GPCRs, have identified residues and contacts that contribute to stability of other proteins.[71,72]

4. CONCLUSIONS

We have computed networks for energy transport in the inactive and active states of β_2AR. Rates of energy transfer between residue pairs are proportional to energy currents between them, which have been computed by using CURrent calculation for Proteins (CURP) developed by Yamato and co-workers.[45] Networks of noncovalent contacts between which rates of energy transfer are relatively large, or energy exchange networks (EENs), appear in both inactive and active states of β_2AR. The EENs include many of the charged residues associated with networks of Class A GPCRs previously[69] as well as contacts including a number of polar as well as some nonpolar interactions. We have found that reorganization of the EENs upon activation reveals a pathway from the agonist-binding pocket to the cytoplasmic, G-protein binding region that includes all the motifs containing molecular switches of β_2AR. The reorganization of EENs for the transition from the inactive to the active state yielding this pathway is quantified by the relative change in rates of energy transfer across noncovalent contacts upon activation.

Changes in EENs upon activation have been shown to reveal pathways for allosteric transitions in other proteins.[7] Here we have compared the reorganization of EENs based on absolute changes in local rates of energy transfer with those based on relative changes. We find that relative changes in rates of energy transfer across noncovalent contacts better capture involvement of van der Waals contacts compared to absolute changes, since rates of energy transfer across van der Waals contacts are relatively small compared to rates across polar contacts and contacts involving charged groups. For this study of β_2AR we find that about half of the largest relative changes in rates of energy transfer across noncovalent contacts occur in motifs, regions that contain molecular switches that mediate activation, and all of the motifs of β_2AR are included in such a mapping of the EEN reorganization. The relative change in an EEN thereby captures structural changes that occur during activation, which is driven thermodynamically. We note that it will be of interest to include water molecules in future work, as water has been shown to contribute to Class A GPCR function and activation.[33,73]

Energy transport networks, and other models that quantify how dynamics at various sites within a protein may be connected,[2−4,6,74] reveal signaling pathways and identify regions that contribute to allosteric transitions. We find that for β_2AR the energy transport networks better capture regions that mediate activation of this protein than distance-based contact networks. While there is some correlation between rates of energy transfer and inter-residue distance, which we have examined, there is sufficient variation that pathways involved in signaling, identified in dynamic networks, are not always captured in a structure-based contact network.

Rates of energy transfer across noncovalent contacts can be measured by a variety of time-resolved spectroscopic techniques.[53,55,57,58] The extent to which the rate of energy transfer across a noncovalent contact varies with change in state or upon mutation can also be probed.[54] The rate of energy transfer is affected by rearrangement of noncovalent contacts as well as by changes in contact dynamics even if the contact itself remains intact.[46−49] Very small adjustments in structure can lead to significant changes in dynamics throughout a protein, with corresponding change in entropy contributing to the thermodynamics of ligand binding and allosteric regulation.[52,75] Changes in contacts accompanying reorganization of energy transport networks, which occur during change of state as illustrated here, as well as in the adaptation to mutation,[76] can thereby be detected by monitoring energy transfer dynamics.

We expect application of dynamic networks to be useful in the computational design of new GPCRs.[77] It will also be of interest to examine the reorganization of energy transport networks in GPCRs of other classes, beyond those of Class A, as more of their structures become available.

■ ASSOCIATED CONTENT

Supporting Information

The Supporting Information is available free of charge at https://pubs.acs.org/doi/10.1021/acs.jpcb.1c03412.

https://doi.org/10.1021/acs.jpcb.1c03412
J. Phys. Chem. B 2021, 125, 6522−6531

Data for energy exchange networks and distance networks (PDF)

AUTHOR INFORMATION

Corresponding Author

David M. Leitner − *Department of Chemistry, University of Nevada, Reno, Nevada 89557, United States;* orcid.org/0000-0002-3105-818X; Email: dml@unr.edu

Author

Humanath Poudel − *Department of Chemistry, University of Nevada, Reno, Nevada 89557, United States*

Complete contact information is available at: https://pubs.acs.org/10.1021/acs.jpcb.1c03412

Notes

The authors declare no competing financial interest.

ACKNOWLEDGMENTS

Support from the NSF (Grant CHE-1854271) is gratefully acknowledged. The authors are grateful to the Cyberinfrastructure Team in the Office of Information Technology at UNR for access to the Pronghorn HPC cluster, with allocation supported by UNR Student Technology Fees.

REFERENCES

(1) DiPaola, L.; Giuliani, A. *Allostery: Methods and Protocols.* Springer: 2021; Vol. *2253*.

(2) Feher, V. A.; Durrant, J. D.; Van Wart, A. T.; Amaro, R. E. Computational Approaches to Mapping Allosteric Pathways. *Curr. Opin. Struct. Biol.* **2014**, *25*, 98−103.

(3) Marcos, E.; Crehuet, R.; Bahar, I. Changes in Dynamics Upon Oligomerization Regulate Substrate Binding and Allostery in Amino Acid Kinese Family Members. *PLoS Comput. Biol.* **2011**, *7*, No. e1002201.

(4) Gheeraert, A.; Pacini, L.; Batista, V. S.; Vuillon, L.; Lesieur, C.; Rivalta, I. Exploring Allosteric Pathways of a V-Type Enzyme with Dynamical Perturbation Networks. *J. Phys. Chem. B* **2019**, *123*, 3452−3461.

(5) Tsai, C.-J.; delSol, A.; Nussinov, R. Protein Allostery, Signal Transmission and Dynamics: A Classification Scheme of Allosteric Mechanisms. *Mol. BioSyst.* **2009**, *5*, 207−216.

(6) Sethi, A.; Eargle, J.; Black, A. A.; Luthey-Schulten, Z. Dynamical Networks in Trna:Protein Complexes. *Proc. Natl. Acad. Sci. U. S. A.* **2009**, *106*, 6620−6625.

(7) Ota, K.; Yamato, T. Energy Exchange Network Model Demonstrates Protein Allosteric Transition: An Application to an Oxygen Sensor Protein. *J. Phys. Chem. B* **2019**, *123*, 768−775.

(8) Leitner, D. M. Energy Flow in Proteins. *Annu. Rev. Phys. Chem.* **2008**, *59*, 233−259.

(9) Leitner, D. M. Water-Mediated Energy Dynamics in a Homodimeric Hemoglobin. *J. Phys. Chem. B* **2016**, *120*, 4019−4027.

(10) Gnanasekaran, R.; Agbo, J. K.; Leitner, D. M. Communication Maps Computed for Homodimeric Hemoglobin: Computational Study of Water-Mediated Energy Transport in Proteins. *J. Chem. Phys.* **2011**, *135*, 065103.

(11) Kong, Y.; Karplus, M. Signaling Pathways of Pdz2 Domain: A Molecular Dynamics Interaction Correlation Analysis. *Proteins: Struct., Funct., Genet.* **2009**, *74*, 145−154.

(12) Leitner, D. M.; Straub, J. E. *Proteins: Energy, Heat and Signal Flow* CRC Press, Taylor & Francis Group: Boca Raton, FL, 2010.

(13) Smock, R. G.; Gierasch, L. M. Sending Signals Dynamically. *Science* **2009**, *324*, 198−203.

(14) Nygaard, R.; Frimurer, T. M.; Holst, B.; Rosenkilde, M. M.; Schwartz, T. W. Ligand Binding and Micro-Switches in 7tm Receptor Structures. *Trends Pharmacol. Sci.* **2009**, *30*, 249−259.

(15) Lee, Y.; Choi, S.; Hyeon, C. Communication of the Network of Binary Switches Regulates the Activation of A2a Adenosine Receptor. *PLoS Comput. Biol.* **2015**, *11*, e1004044.

(16) Trzaskowski, B.; Latek, D.; Yuan, S.; Ghoshdastider, U.; Debinski, A.; Filipek, S. Action of Molecular Switches in Gpcrs - Theoretical and Experimental Studies. *Curr. Med. Chem.* **2012**, *19*, 1090−1109.

(17) Dror, R. O.; Arlow, D. H.; Borhani, D. W.; Jensen, M.; Piana, S.; Shaw, D. E. Identification of Two Distinct Inactive Conformations of the B 2-Adrenergic Receptor Reconciles Structural and Biochemical Observations. *Proc. Natl. Acad. Sci. U. S. A.* **2009**, *106*, 4689−4694.

(18) Latorraca, N. R.; Venkatakrishnan, A. J.; Dror, R. O. Gpcr Dynamics: Structures in Motion. *Chem. Rev.* **2017**, *117*, 139−155.

(19) Manglik, A.; Kim, T. H.; Masureel, M.; Altenbach, C.; Yang, Z.; Hilger, D.; Lerch, M. T.; Kobilka, T. S.; Thian, F. S.; Hubbell, W. L.; et al. Structural Insights into the Dynamic Process of Beta2-Adrenergic Receptor Signaling. *Cell* **2015**, *161*, 1101−1111.

(20) Rosenbaum, D. M.; Rasmussen, S. G. F.; Kobilka, B. K. The Structure and Function of G-Protein-Coupled Receptors. *Nature* **2009**, *459*, 356−363.

(21) Huang, S. K.; Pandey, A.; Tran, D. P.; Villanueva, N. L.; Kitao, A.; Sunahara, R. K.; Sljoka, A.; Prosser, R. S. Delineating the Conformational Landscape of the Adenosine A2a Receptor During G Protein Coupling. *Cell* **2021**, *184*, 1884−1894.

(22) Tuteja, N. Signaling through G Protein Coupled Receptors. *Plant Signaling Behav.* **2009**, *4*, 942−947.

(23) Rasmussen, S. G. F.; Devree, B. T.; Zou, Y.; Kruse, A. C.; Chung, K. Y.; Kobilka, T. S.; Thian, F. S.; Chae, P. S.; Pardon, E.; Calinski, D.; et al. Crystal Structure of the B2 Adrenergic Receptor-G Protein Complex. *Nature* **2011**, *477*, 549−557.

(24) Lefkowitz, R. J. The Superfamily of Heptahelical Receptors. *Nat. Cell Biol.* **2000**, *2*, E133−E136.

(25) DiPaola, L.; Giuliani, A. Protein Contact Network Topology: A Natural Language for Allostery. *Curr. Opin. Struct. Biol.* **2015**, *31*, 43−48.

(26) DiPaola, L.; DeRuvo, M.; Paci, P.; Santoni, D.; Giuliani, A. Protein Contact Networks: An Emerging Paradigm in Chemistry. *Chem. Rev.* **2013**, *113*, 1598−1613.

(27) Lee, Y.; Choi, S.; Hyeon, C. Mapping the Intramolecular Signal Transduction of G-Protein Coupled Receptors. *Proteins: Struct., Funct., Genet.* **2014**, *82*, 727−743.

(28) Karathanou, K.; Lazaratos, M.; Bertalan, É.; Siemers, M.; Buzar, K.; Schertler, G. F. X.; DelVal, C.; Bondar, A.-N. A Graph-Based Approach Identifies Dynamic H-Bond Communication Networks in Spike Protein S of Sars-Cov-2. *J. Struct. Biol.* **2020**, *212*, 107617.

(29) Leitner, D. M.; Yamato, T. Recent Developments in the Computational Study of Protein Structural and Vibrational Energy Dynamics. *Biophys. Rev.* **2020**, *12*, 317−322.

(30) Leitner, D. M.; Yamato, T.; Parrill, A. L.; Lipkowitz, K. B. Mapping Energy Transport Networks in Proteins. *Rev. Comput. Chem.* **2018**, *31*, 63−113.

(31) Lazaratos, M.; Karathanou, K.; Bondar, A.-N. Graphs of Dynamic H-Bond Networks: From Model Proteins to Protein Complexes in Cell Signaling. *Curr. Opin. Struct. Biol.* **2020**, *64*, 79−87.

(32) Leitner, D. M.; Hyeon, C.; Reid, K. M. Water-Mediated Biomolecular Dynamics and Allostery. *J. Chem. Phys.* **2020**, *152*, 240901.

(33) Lee, Y.; Kim, S.; Choi, S.; Hyeon, C. Ultraslow Water-Mediated Transmembrane Interactions Regulate the Activation of A2a Adenosine Receptor. *Biophys. J.* **2016**, *111*, 1180−1191.

(34) Gnanasekaran, R.; Xu, Y.; Leitner, D. M. Dynamics of Water Clusters Confined in Proteins: A Molecular Dynamics Simulation Study of Interfacial Waters in a Dimeric Hemoglobin. *J. Phys. Chem. B* **2010**, *114*, 16989−16996.

(35) Ishikura, T.; Yamato, T. Energy Transfer Pathways Relevant for Long-Range Intramolecular Signaling of Photosensory Protein Revealed by Microscopic Energy Conductivity Analysis. *Chem. Phys. Lett.* **2006**, *432*, 533−537.

(36) Xu, Y.; Leitner, D. M. Vibrational Energy Flow through the Green Fluorescent Protein-Water Interface: Communication Maps and Thermal Boundary Conductance. *J. Phys. Chem. B* **2014**, *118*, 7818−7826.
(37) Agbo, J. K.; Gnanasekaran, R.; Leitner, D. M. Communication Maps: Exploring Energy Transport through Proteins and Water. *Isr. J. Chem.* **2014**, *54*, 1065−1073.
(38) Leitner, D. M. Frequency Resolved Communication Maps for Proteins and Other Nanoscale Materials. *J. Chem. Phys.* **2009**, *130*, 195101.
(39) Agbo, J. K.; Xu, Y.; Zhang, P.; Straub, J. E.; Leitner, D. M. Vibrational Energy Flow across Heme-Cytochrome C and Cytochrome C-Water Interfaces. *Theor. Chem. Acc.* **2014**, *133*, 1504.
(40) Leitner, D. M.; Buchenberg, S.; Brettel, P.; Stock, G. Vibrational Energy Flow in the Villin Headpiece Subdomain: Master Equation Simulations. *J. Chem. Phys.* **2015**, *142*, 075101.
(41) Leitner, D. M. Heat Transport in Proteins. In *Proteins: Energy, Heat and Signal Flow*; Leitner, D. M., Straub, J. E., Eds.; Taylor and Francis: New York, 2010; pp 247−270.
(42) Yu, X.; Leitner, D. M. Vibrational Energy Transfer and Heat Conduction in a Protein. *J. Phys. Chem. B* **2003**, *107*, 1698−1707.
(43) Yu, X.; Leitner, D. M. Heat Flow in Proteins: Computation of Thermal Transport Coefficients. *J. Chem. Phys.* **2005**, *122*, 054902.
(44) Leitner, D. M. Heat Transport in Molecules and Reaction Kinetics: The Role of Quantum Energy Flow and Localization. *Adv. Chem. Phys.* **2005**, *130B*, 205−256.
(45) Ishikura, T.; Iwata, Y.; Hatano, T.; Yamato, T. Energy Exchange Network of Inter-Residue Interactions within a Thermally Fluctuating Protein: A Computational Study. *J. Comput. Chem.* **2015**, *36*, 1709−1718.
(46) Reid, K. M.; Yamato, T.; Leitner, D. M. Variation of Energy Transfer Rates across Protein-Water Contacts with Equilibrium Structural Fluctuations of a Homodimeric Hemoglobin. *J. Phys. Chem. B* **2020**, *124*, 1148−1159.
(47) Reid, K. M.; Yamato, T.; Leitner, D. M. Scaling of Rates of Vibrational Energy Transfer in Proteins with Equilibrium Dynamics and Entropy. *J. Phys. Chem. B* **2018**, *122*, 9331−9339.
(48) Poudel, H.; Reid, K. M.; Yamato, T.; Leitner, D. M. Energy Transfer across Nonpolar and Polar Contacts in Proteins: Role of Contact Fluctuations. *J. Phys. Chem. B* **2020**, *124*, 9852−9861.
(49) Leitner, D. M.; Pandey, H. D.; Reid, K. M. Energy Transport across Interfaces in Biomolecular Systems. *J. Phys. Chem. B* **2019**, *123*, 9507−9524.
(50) Buchenberg, S.; Leitner, D. M.; Stock, G. Scaling Rules for Vibrational Energy Transport in Proteins. *J. Phys. Chem. Lett.* **2016**, *7*, 25−30.
(51) Valino-Borau, L.; Gulzar, A.; Stock, G. Master Equation Model to Preduct Energy Transport Pathways in Proteins. *J. Chem. Phys.* **2020**, *152*, 045103.
(52) Reid, K. M.; Yu, X.; Leitner, D. M. Change in Vibrational Entropy with Change in Protein Volume Estimated with Mode GrüNeisen Parameters. *J. Chem. Phys.* **2021**, *154*, 055102.
(53) Mizuno, M.; Mizutani, Y. Role of Atomic Contacts in Vibrational Energy Transfer in Myoglobin. *Biophys. Rev.* **2020**, *12*, 511−518.
(54) Yamashita, S.; Mizuno, M.; Tran, D. P.; Dokainish, H.; Kitao, A.; Mizutani, Y. Vibrational Energy Transfer from Heme through Atomic Contacts in Proteins. *J. Phys. Chem. B* **2018**, *122*, 5877−5884.
(55) Mizutani, Y. Time-Resolved Resonance Raman Spectroscopy and Application to Studies on Ultrafast Protein Dynamics. *Bull. Chem. Soc. Jpn.* **2017**, *90*, 1344−1371.
(56) Fujii, N.; Mizuno, M.; Ishikawa, H.; Mizutani, Y. Observing Vibrational Energy Flow in a Protein with the Spatial Resolution of a Single Amino Acid Residue. *J. Phys. Chem. Lett.* **2014**, *5*, 3269−3273.
(57) Baumann, T.; Hauf, M.; Schildhauer, F.; Eberl, K. B.; Durkin, P. M.; Deniz, E.; Löffler, J. G.; Acevedo-Rocha, C. G.; Jaric, J.; Martins, B. M.; et al. Observation of Site-Resolved Vibrational Energy Transfer Using a Genetically Encoded Ultrafast Heater. *Angew. Chem., Int. Ed.* **2019**, *58*, 2899−2903.
(58) Müller-Werkmeister, H. M.; Bredenbeck, J. A Donor-Acceptor Pair for the Real Time Study of Vibrational Energy Transfer in Proteins. *Phys. Chem. Chem. Phys.* **2014**, *16*, 3261−3266.
(59) Fiser, A.; Sali, A. Modloop: Automated Modeling of Loops in Protein Structures. *Bioinformatics* **2003**, *19*, 2500−2501.
(60) Allouche, A. Software News and Updates Gabedit — a Graphical User Interface for Computational Chemistry Softwares. *J. Comput. Chem.* **2011**, *32*, 174−182.
(61) Maier, J. A.; Martinez, C.; Kasavajhala, K.; Wickstrom, L.; Hauser, K. E.; Simmerling, C. Ff14sb: Improving the Accuracy of Protein Side Chain and Backbone Parameters from Ff99sb. *J. Chem. Theory Comput.* **2015**, *11*, 3696−3713.
(62) Dickson, C. J.; Madej, B. D.; Skjevik, Å. A.; Betz, R. M.; Teigen, K.; Gould, I. R.; Walker, R. C. Lipid14: The Amber Lipid Force Field. *J. Chem. Theory Comput.* **2014**, *10*, 865−879.
(63) Berendsen, H. J. C.; Postma, J. P. M.; van Gunsteren, W. F.; DiNola, A.; Haak, J. R. Molecular Dynamics with Coupling to an External Bath. *J. Chem. Phys.* **1984**, *81*, 3684−3690.
(64) Yamato, T. Energy Flow Pathways in Photoreceptor Proteins. In *Proteins: Energy, Heat and Signal Flow*; Leitner, D. M., Straub, J. E., Eds.; CRC Press: Boca Raton, FL, 2010; pp 129−147.
(65) Ballesteros, J. A.; Weinstein, H. Integrated Methods for the Construction of Three-Dimensional Models and Computational Probing of Structure-Function Relations in G Protein-Coupled Receptors. *Methods Neurosci.* **1995**, *25*, 366−428.
(66) Yamato, T.; Higo, J.; Seno, Y.; Go, N. Conformational Deformation in Deoxymyoglobin by Hydrostatic Pressure. *Proteins: Struct., Funct., Genet.* **1993**, *16*, 327−340.
(67) Dror, R. O.; Arlow, D. H.; Maragakis, P.; Mildorf, T. J.; Pan, A. C.; Xu, H.; Borhani, D. W.; Shaw, D. E. Activation Mechanism of the B 2-Adrenergic Receptor. *Proc. Natl. Acad. Sci. U. S. A.* **2011**, *108*, 18684−18689.
(68) Saleh, N.; Saladino, G.; Gervasio, F. L.; Clark, T. Investigating Allosteric Effects on the Functional Dynamics of B2-Adrenergic Ternary Complexes with Enhanced-Sampling Simulations. *Chem. Sci.* **2017**, *8*, 4019−4026.
(69) Isom, D. G.; Dohlman, H. G. Buried Ionizable Networks Are an Ancient Hallmark of G Protein-Coupled Receptor Activation. *Proc. Natl. Acad. Sci. U. S. A.* **2015**, *112*, 5702−5707.
(70) Venkatakrishnan, A. J.; Deupi, X.; Lebon, G.; Tate, C. G.; Schertler, G. F.; Babu, M. M. Molecular Signatures of G-Protein-Coupled Receptors. *Nature* **2013**, *494*, 185−194.
(71) Achoch, M.; Dorantes-Gilardi, R.; Wymant, C.; Feverati, G.; Salamatian, K.; Vuillon, L.; Lesieur, C. Protein Structural Robustness to Mutations: An in Silico Investigation. *Phys. Chem. Chem. Phys.* **2016**, *18*, 13770−13780.
(72) Vuillon, L.; Lesieur, C. From Local to Global Changes in Proteins: A Network View. *Curr. Opin. Struct. Biol.* **2015**, *31*, 1−8.
(73) Angel, T. E.; Chance, M. R.; Palczewski, K. Conserved Waters Mediate Structural and Functional Activation of Family a (Rhodopsin-Like) G Protein-Coupled Receptors. *Proc. Natl. Acad. Sci. U. S. A.* **2009**, *106*, 8555−8560.
(74) Rivalta, I.; Batista, V. S. Community Network Analysis of Allosteric Proteins. *Methods Mol. Biol.* **2021**, *2253*, 137−151.
(75) Bozovic, O.; Zanobini, C.; Gulzar, A.; Jankovic, B.; Buhrke, D.; Post, M.; Wolf, S.; Stock, G.; Hamm, P. Real-Time Observation of Ligand-Induced Allosteric Transitions in a PDZ Domain. *Proc. Natl. Acad. Sci. U. S. A.* **2020**, *117*, 26031−26039.
(76) Leander, M.; Yuan, Y.; Meger, A.; Cui, Q.; Raman, S. Functional Plasticity and Evolutionary Adaptation of Allosteric Regulation. *Proc. Natl. Acad. Sci. U. S. A.* **2020**, *117*, 25445−25454.
(77) Chen, K.-Y. M.; Keri, D.; Barth, P. Computational Design of G Protein-Coupled Receptor Allosteric Signal Transductions. *Nat. Chem. Biol.* **2020**, *16*, 77−86.

https://doi.org/10.1021/acs.jpcb.1c03412
J. Phys. Chem. B 2021, 125, 6522−6531